

STRAY-LIGHT CORRECTION IN MAGNETOGRAPH OBSERVATIONS USING THE MAXIMUM ENTROPY METHOD

JONGCHUL CHAE¹, HONG SIK YUN², TAKASHI SAKURAI³ and KIYOSHI
ICHIMOTO³

¹*Big Bear Solar Observatory, New Jersey Institute of Technology, 40386 North Shore Lane, Big
Bear City, CA 92314, U.S.A.*

²*Department of Astronomy, Seoul National University, Seoul 151-742, Korea*

³*National Astronomical Observatory, Mitaka, Tokyo 181, Japan*

(Received 19 June 1998; accepted 17 July 1998)

Abstract. We have developed a method of stray-light correction which is applicable to filter-based magnetograph observations. Stray-light-corrected Stokes images are obtained by performing the deconvolution of observed Stokes images by the point spread function which is determined from the Stokes *I* image. For image deconvolution, the maximum entropy principle is used to guarantee that intensity should be positive and polarization degrees should be less than unity. We present an iterative algorithm for the maximum entropy method, which seeks the solution in Fourier space and thus accomplishes fast convergence. We find that our method is effective in correcting stray light which has a spread angle greater than the full width at half maximum of the point spread function. We also discuss the effect of stray light on magnetograph calibration.

1. Introduction

We have examined the stray-light effect on magnetograph observations in our previous work (Chae *et al.*, 1998, hereafter Paper I). As a result, we find that small spread-angle stray light disturbs polarization measurements of small magnetic features like pores and network elements, whereas large spread-angle stray light leads to an underestimation of polarization in dark magnetic features like sunspot umbrae. In the present work, we develop a method of correction for both small and large spread-angle stray light which is applicable to magnetograph observations.

The correction for stray light is basically a process of image deconvolution – which is to determine the disturbance-free intrinsic images from the observed images. In solar observations, most effort has been made to correct for large spread-angle stray light which is produced by scattering in the instrument and the Earth's atmosphere. This kind of effort is important especially in determining sunspot intensity. The traditional method for the correction of large spread-angle stray light is relatively simple. Once the scattered light integral is known as a function of distance from the disk center, it is subtracted from the observed intensity, and the result is divided by a suitable normalizing factor to give the corrected intensity (Wittmann and Wöhl, 1975). This traditional approach works well for stray light



characterized by a spread angle much greater than about $20''$. However, it cannot be applicable to the correction of smaller spread-angle stray light, since the intrinsic intensity distribution is not known accurately enough to be used for the calculation of the small spread-angle stray light integral before the stray-light correction is made. Martinez Pillet (1992) partially overcame this difficulty by introducing an iterative correction scheme. He initially assumed an intrinsic intensity distribution. The stray-light integral was then calculated at every point by convolving the intrinsic distribution with the point spread function, and was subtracted from the observed intensity to obtain a new estimate of intrinsic intensity distribution. The same process was repeated until it converged. This scheme was used to correct for stray light with a spread angle greater than $10''$. However, correction for even smaller spread-angle stray light is not an easy task, since a deconvolution may cause small-scale artifacts due to noise.

During the last two decades, numerous algorithms for image deconvolution have been developed, which are intended to reveal small scale true features while suppressing artifacts. They include Wiener filtering (Brault and White, 1971), the Richardson–Lucy method (Richardson, 1972; Lucy, 1974), CLEAN algorithm (Högbom, 1974) and the maximum entropy method (Skilling and Bryan, 1984; Narayan and Nityananda, 1986). Among them, we choose the maximum entropy method for our purpose since its principle is now well established and known to be effective in suppressing noisy features. The regularizing capability of this principle mainly comes from the introduction of the so-called entropy term which assures the positivity of intensity in the deconvolved image. In the present work, we apply this principle to correct for stray light in polarization measurements.

2. Mathematical Formulation

We will work only with a pair of Stokes I and V images, but the following formulations are straightforward applicable to Q and U images, too. In Paper I, we have decomposed Stokes I into the center-to-limb background component I_{bg} and the residual component I_{re} , and decomposed the point spread function into the blurring part $(1 - \epsilon)\psi_{\text{bl}}$, and the scattering part $\epsilon\psi_{\text{sc}}$. Here ϵ is the scattered light fraction at disk center. Then we have obtained the following equations:

$$I_{\text{re}}^{\text{obs}} = (1 - \epsilon)I_{\text{re}}^* , \quad (1)$$

$$V^{\text{obs}} = (1 - \epsilon)V^* , \quad (2)$$

$$I_{\text{bg}}^{\text{obs}} = (1 - \epsilon)I_{\text{bg}}^* + \epsilon S , \quad (3)$$

where the superscripts $*$ denote the convolution with the blurring function ψ_{bl} , and S is the normalized scattered-light integral defined by

$$S = I_{\text{bg}} * \psi_{\text{sc}} . \quad (4)$$

All the Stokes images and point spread functions are normalized to satisfy

$$I_{\text{bg}} = I_{\text{bg}} * \psi_{\text{bl}} = I_{\text{bg}} * \psi_{\text{sc}} = 1 \quad (5)$$

at disk center. How to determine ψ_{bg} , ψ_{sc} , ϵ , and S from observations has been described in Paper I. Here we assume that they are all known.

It is straightforward to correct I_{re} , V , and I_{bg} for large spread-angle stray light described by ϵ and ψ_{sc} :

$$I_{\text{re}}^* = \frac{I_{\text{re}}^{\text{obs}}}{1 - \epsilon}, \quad (6)$$

$$V^* = \frac{V^{\text{obs}}}{1 - \epsilon}, \quad (7)$$

$$I_{\text{bg}}^* = \frac{I_{\text{bg}}^{\text{obs}} - \epsilon S}{1 - \epsilon}. \quad (8)$$

Therefore, the polarization corrected for large spread-angle stray light is given by

$$\frac{V^*}{I^*} = \frac{V^{\text{obs}}}{I^{\text{obs}} - \epsilon S}, \quad (9)$$

where $I^* = I_{\text{re}}^* + I_{\text{bg}}^*$ and $I^{\text{obs}} = I_{\text{re}}^{\text{obs}} + I_{\text{bg}}^{\text{obs}}$. The integral S is a function of distance from disk center which monotonically decreases from unity at disk center to zero at infinity. An example of calculated S is provided in Paper I. In case of disk observations not far from disk center, it is approximately equal to unity so that specific information on the functional form of S is not required. This means that it is enough to know only one parameter ϵ for the correction of large spread-angle stray light in disk observations.

On the other hand, the correction for small spread-angle stray light is not trivial. We first assume that $I_{\text{bg}} = I_{\text{bg}} * \psi_{\text{bl}}$, since I_{bg} varies very slowly over the solar surface. Then it remains to obtain I_{re} and V from I_{re}^* and V^* . The solution of I_{re} and V should satisfy two basic physical constraints: the total intensity should be positive and the absolute value of the polarization degree should be less than unity. These constraints play a role in getting physically plausible I and V from image deconvolution, and have been applied to a maximum entropy reconstruction of the polarized brightness distribution from interferometric radio observations (Nityananda and Narayan, 1983). Basically, these constraints are a consequence of the fundamental requirement that the intensity of any light component should be positive irrespective of its polarization status as is shown below. The necessary and sufficient conditions for these constraints are

$$I_{\text{re}} \pm V + I_{\text{bg}} > 0. \quad (10)$$

If we introduce two new variables I_+ and I_- defined by

$$I_{\pm} = I_{\text{re}} \pm V, \quad (11)$$

then the problem is reduced to find I_{\pm} which satisfies

$$I_{\pm} * \psi_{\text{bl}} = \frac{I_{\text{re}}^{\text{obs}} \pm V^{\text{obs}}}{1 - \epsilon} \quad (12)$$

under the constraint

$$I_{\pm} = I_{\text{bg}} > 0. \quad (13)$$

The following section addresses this kind of problem based on the maximum entropy principle.

3. Maximum Entropy Method

The goal of this section is to determine a two-dimensional distribution $x(\mathbf{r})$ which satisfies

$$y(\mathbf{r}) = x(\mathbf{r})f(\mathbf{r}) \quad (14)$$

for given distributions of $y(\mathbf{r})$ and $f(\mathbf{r})$ under the constraint

$$a(\mathbf{r})x(\mathbf{r}) + b(\mathbf{r}) > 0 \quad (15)$$

with specified distributions $a(\mathbf{r})$ and $b(\mathbf{r})$. For the determination of the solution $x(\mathbf{r})$, the maximum entropy principle uses a Bayesian approach which maximizes the function

$$H = \alpha S + L, \quad (16)$$

where S is the entropy which is a measure of the solution's compatibility with a priori information, and L is the likelihood which is a measure of the solution's fitness to data. The free parameter α , a regularizing parameter, determines the weights of the two terms.

According to Skilling (1989), the entropy can be used as a measure of the prior probability for any positive and additive quantities. Thus we introduce a positive-definite variable

$$z(\mathbf{r}) \equiv a(\mathbf{r})x(\mathbf{r}) + b(\mathbf{r}) \quad (17)$$

and define the entropy of the solution like

$$S = \sum_s (z_s - m_s - z_s \log(z_s/m_s)), \quad (18)$$

where the subscript s denotes the index number of discrete data points in the spatial domain. The functional form of the entropy has been taken from Gull (1989) and Skilling (1990). The default image m_s can be freely chosen as input. We set it to be equal to $a_s y_s + b_s$. We find that it is convenient to define the likelihood in the Fourier domain,

$$L = -\frac{c}{2} \sum_n |X_n F_n - Y_n|^2, \quad (19)$$

where X , F , and Y are the Fourier transforms of x , f , and y , respectively. The subscript n represents the index number of discrete data points in the Fourier domain. The constant c is a free parameter introduced to guarantee that the regularizing parameter is dimensionless by forcing L to have the same physical dimension as S .

In Appendix A, we derived the following iterative formula for x_s , or equivalently, X_n which maximizes H :

$$X_n^{(k+1)} = \frac{Y_n F_n^* + \alpha(\lambda^{(k)} X_n^{(k)} - Q_n^{(k)})}{|F_n|^2 + \alpha\lambda^{(k)}}, \quad (20)$$

where the definitions $Q_n^{(k)}$ and $\lambda^{(k)}$ are given in Appendix A as well as how to calculate them. The detailed numerical algorithm using this formula is described in Appendix B. This formal solution illustrates how the maximum entropy method works in the deconvolution process. If it were not for the second term in the numerator, $\alpha(\lambda^{(k)} X_n^{(k)} - Q_n^{(k)})$, the solution would have the same form as the well-known Wiener filter. The second term in the denominator $\alpha\lambda^{(k)}$ suppresses high-frequency noise, and it is equivalent to the noise-to-signal power ratio in the Wiener filter. Note that this term has a real value so that it affects only the amplitude of the complex solution X_n , but has no effect on its phase. The unique characteristic of the maximum entropy method comes from the second term in the numerator. This term is complex and non-linear to X_n and x_s . This nonlinear term couples high and low frequency information, and suppresses noisy features while keeping real features. In some special cases, low-frequency information can be extrapolated to high-frequency information even beyond the cut-off frequency imposed by observations to obtain super-resolution (Narayan and Nityananda, 1986).

4. Applications

We apply our method of stray-light correction to the vector magnetograph observations of the active region NOAA 7260 performed by the Japanese Solar Flare Telescope on 18 August 1992. Figures 1 and 4 show the Stokes I and V/I images taken on that day. A full description of the telescope has been given by Sakurai *et al.* (1995). Paper I described the observations and data reduction, and determined the point spread function using the intensity power spectrum method. As a result,

it was found that the blurring part of the point spread function on this day is given by a Moffat function

$$\psi_{\text{bl}} = \frac{a}{2\pi(r^2 + a^2)^{3/2}} \quad (21)$$

with $a = 1.5''$. Note that the Fourier transform of this function is given by $\exp(-ak)$. Another important parameter which is necessary for stray-light correction is the scattered light fraction ϵ . However, we do not know ϵ , since there was no limb observation made on that day, which can be used for accurate determination of ϵ . What is known from the previous work is that ϵ typically has a value between 10 and 20% on clear days. Since the present observations were obtained on a fairly clear day, we expect that ϵ in our observations may be relatively small. The features most sensitive to the precise value of ϵ are the umbral regions of large sunspots. We have chosen $\epsilon = 0.10$, which makes the intensity of the large sunspot umbra after stray light correction nearly equal to 0.1, which, is a typical umbral brightness (Maltby, 1992). To apply the maximum entropy method, we have selected $\alpha = 10^{-2}$, which is comparable to the ratio of noise power to signal power we estimated from the analysis of power spectrum of Stokes I image.

Figure 1 presents the comparison between the raw Stokes I image without stray light correction and the restored image. It is obvious that the restored image has a higher intensity contrast and reveals small scale structures better than the raw image. Before we make detailed comparisons between the two, we first address the following question: how effective is our image reconstruction in correcting for stray light and suppressing artifacts? For this purpose, we examine the point spread function of the restored image. An ideal image reconstruction algorithm should guarantee that the point spread function of the restored image be a δ -function. But in real situations, because of noise in the data and artifacts arising from numerical procedures, this ideal never occurs. We determined the point spread function of the restored image using the intensity power spectrum method described in Paper I. Figure 2 presents the modulation transfer function and point spread function of the restored image. For comparison, we also provided the corresponding functions of the raw image. From Figure 2(a), we see that the restoration has been done in a way which increases the amplitudes of the Fourier modes with wave numbers at which noise is negligible, and to reduce those with high wave numbers where noise dominates. These characteristics of Fourier amplitude at lower and higher wave numbers explain why the restored image has higher intensity contrast while appearing less noisy. However, these characteristics result in a rapid decrease of Fourier amplitude from low to high wave numbers which may cause an artifact called Gibbs oscillations. This problem is well illustrated in Figure 2(b). Namely, the point spread function of the restored image has a side lobe of a negative value. This is unphysical because the point spread function is a kind of probability function describing the redistribution of intensity, which should be positive by definition. The side lobe is manifest in a restored image as either a dark ring around a bright point source or a

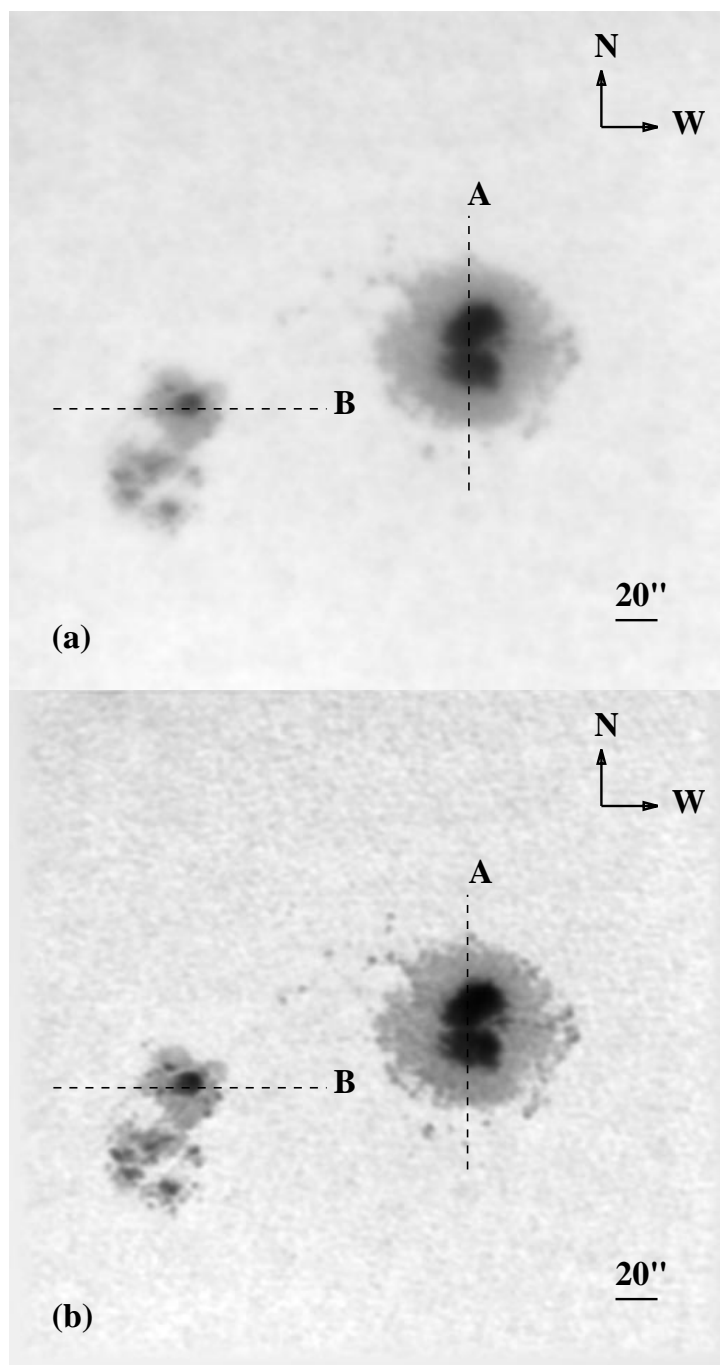


Figure 1. (a) Raw Stokes I image of AR 7260 on 18 August 1992. (b) Stray-light-corrected Stokes I image. The images have been apodized at the boundaries to minimize the edge effect on image deconvolution. The field of view is $350'' \times 330''$.

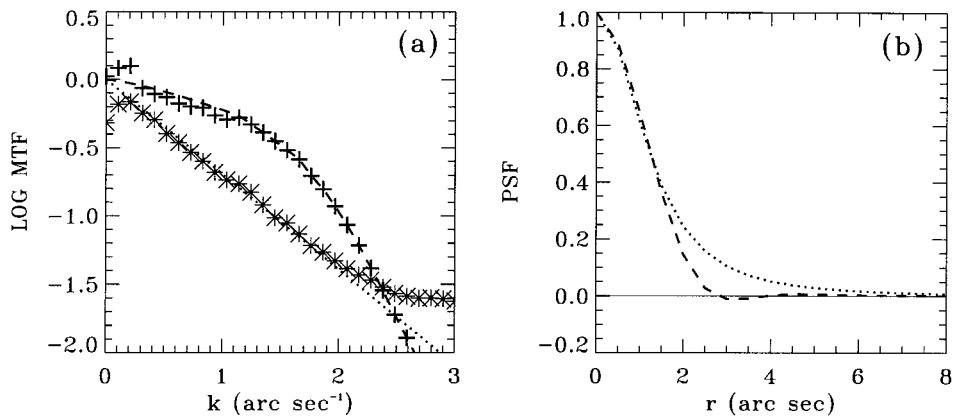


Figure 2. (a) Modulation transfer functions (asterisks: raw image; + marks: corrected image). The dotted curve is the MTF of the raw image after correction for noise. (b) Point spread functions (dotted curve: raw image; dashed curve: corrected image).

bright ring around a dark point source. The side lobe could be removed by picking a larger value of the regularizing parameter α for image deconvolution, but, in this case, the stray light with smaller spread angle is not effectively corrected. In the present analysis, we have used $\alpha = 10^{-2}$. This choice limits the depth of the side lobe within 2% of the peak value of the point spread function, which is considered to be tolerable for our purpose. As seen from Figure 2(b), the image restoration based on this choice affects mainly the wing of the point spread function, with little effect on the central part. This means that even though our stray light correction only slightly improved the spatial resolution of the data, it was successful in correcting for the stray light with a spread angle greater than the FWHM value of $2.3''$.

For a quantitative comparison between the raw and restored images, we present in Figure 3 the one-dimensional intensity distributions along the line segments A and B, which are profiles of two large sunspots in the active region. As seen from Figure 3(a), the intensity of the very large sunspot umbra which is corrected for both scattering and blurring is not much different from that which is corrected for scattering only. This means that the intensity at the umbral region of a very large sunspot is much more affected by large spread-angle stray light (scattering) than by small spread-angle stray light (blurring). On the other hand, as can be seen from the satellite spot located at $Y = 45''$ in Figure 3(a), a small spot is much more affected by small spread-angle stray light (blurring) than large spread-angle stray light (scattering). Figure 3(b) shows that the intensity even at the umbra of a relative large sunspot is disturbed by small spread-angle stray light unless the spot is large enough. Note that the spots shown in Figures 3(a) and 3(b) have umbral radii of $25''$ and $10''$, respectively, which are much larger than the point spread function FWHM value of $2.3''$. From the result that the smaller spot with the umbral radius of $10''$ is

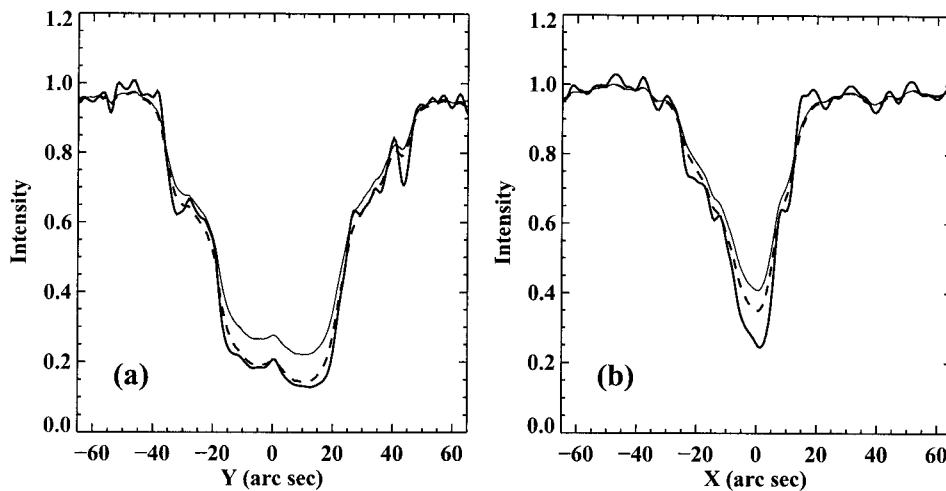


Figure 3. (a) Stokes I profile of the line segment A. (b) Stokes I profile of the line segment B. Thin solid curves: raw data, dashed curves: corrected for scattering only, thick solid curves: corrected for both scattering and blurring.

significantly affected by small spread-angle stray light whereas the larger spot with the umbral radius of $25''$ is little affected by it, we see that the small spread-angle stray light with a spread angle in the range between $2''$ and $20''$ is important in most sunspots other than very large sunspots.

Figure 4 presents the raw and corrected V/I images. As in the case of Stokes I images, the stray light corrected image displays fine structures with a higher contrast than the raw image. In particular, the restored image clearly shows that the magnetic flux outside the sunspots exists in highly concentrated forms. To examine in detail the stray-light effect in polarization measurement, we presented in Figure 5 the raw and corrected V/I distributions along the line segments A and B. Understanding how stray light affects the measurements of polarization in sunspots is much more difficult than understanding the effect of stray light on intensity measurements, since the polarization given by V/I depends on both V and I , and the distribution of V in sunspots is more complicated than that of I .

Figure 5(a) shows that in the penumbra of the large sunspot the V/I profile corrected for both blurring and scattering deviates little from that corrected for scattering only. This indicates that the polarization measurement in this part is mainly affected by large spread-angle stray light. In the umbra of this spot, however, the V/I profile corrected for both blurring and scattering is much different from that corrected for scattering only. This means that polarization measurement in the umbra is affected not only by scattering but also by blurring, unlike the case of intensity measurement. This is attributed to the fact that the umbral region emits such a small amount of polarized light that it is easily polluted by polarized stray light coming from the penumbra. There are two reasons why the amount

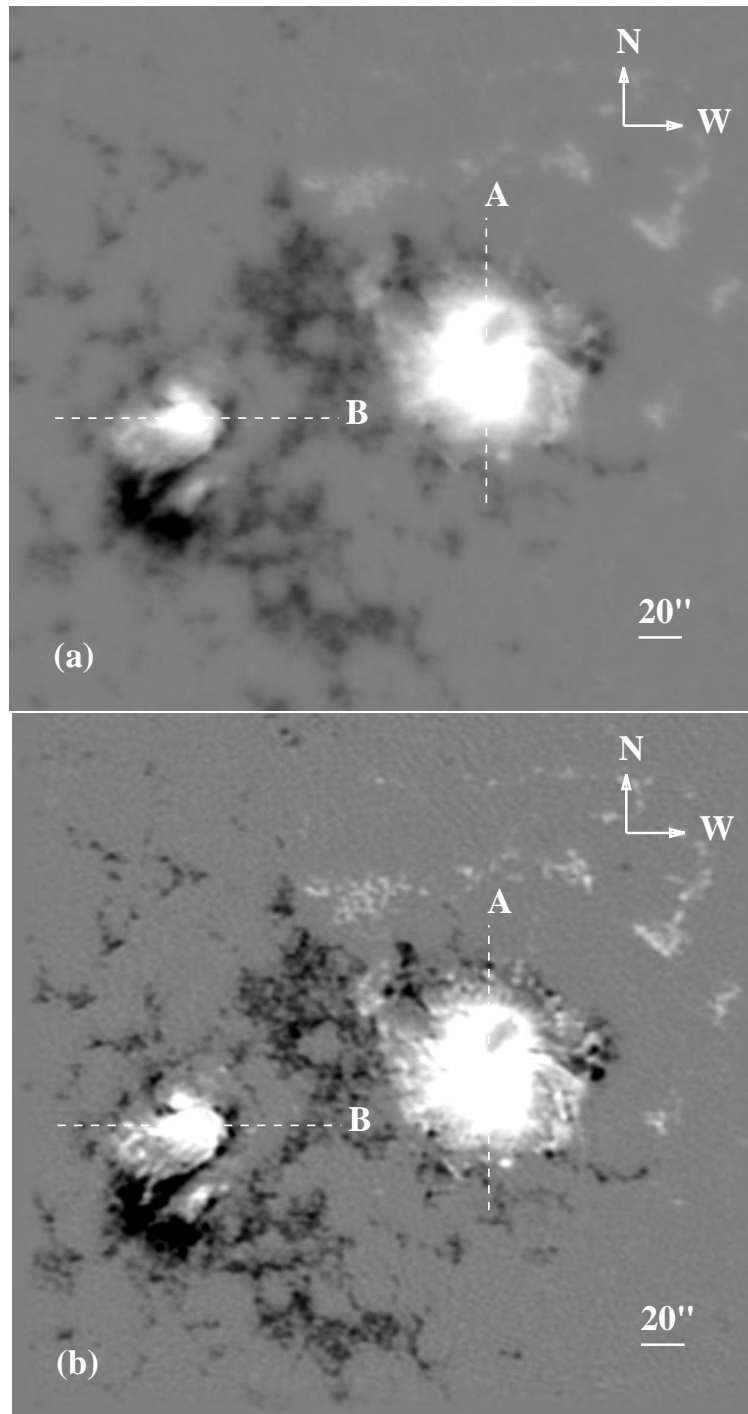


Figure 4. (a) Raw V/I image. (b) Stray-light-corrected Stokes V/I image.

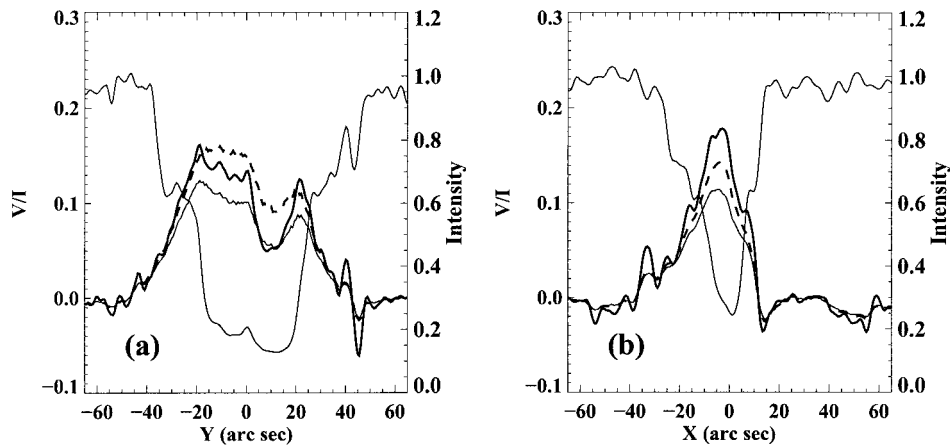


Figure 5. (a) V/I profile of the line segment A. (b) V/I profile of the line segment B.

of polarized light intrinsically emitted by the umbra is so small. First, it has a very low intrinsic intensity. Second, since the field strength is very strong, the line splitting becomes so large that the polarization at the fixed wavelength position is no longer linear to magnetic field strength and even decreases with field strength (called polarization reversal), resulting in a smaller value of polarization degree. This complicated situation is very specific to the umbrae of very large sunspots. But in most sunspots, both blurring and scattering cause the degree of polarization to be underestimated, as demonstrated in Figure 5(b).

5. Stray-Light Effect on Magnetograph Calibration

We examine how stray light affects magnetograph calibration. One of the methods which convert measured polarizations to magnetic field strengths makes use of theoretical calibration curves constructed from solutions of radiative transfer in model magnetized atmospheres. However, directly applying theoretical calibration curves to measured polarizations often produces magnetic field strengths which are seriously underestimated since the measured polarizations may appear less than theoretically expected ones because of instrumental problems. Thus measured polarizations are often multiplied by a simple factor, called k -factor, to come up with reasonable estimates of field strength. A typical value of k -factor adopted for the Marshall Space Flight Center vector magnetograph is about 4 (Gary, Hagyard and West, 1991). The present study shows that stray light is one of the sources which are responsible for depolarization. Therefore, it is worthwhile to determine k -factors for the raw data and stray-light-corrected data, respectively, and compare the two values.

For this purpose, we make use of the largest sunspot in the active region (see Figure 1) as a reference. Skumanich (1992) showed that a round spot may be repre-

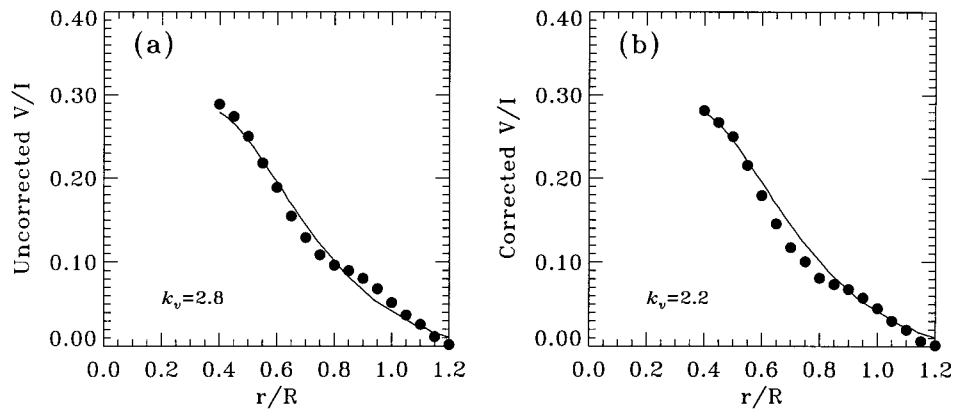


Figure 6. (a) Radial distribution of raw V/I data, which has been multiplied by a factor of 2.8. (b) Radial distribution of stray-light-corrected V/I data, which has been multiplied by a factor of 2.2. The solid curve represents the theoretically expected polarization.

sented quite well by a buried dipole. According to this representation, the magnetic field distribution in a sunspot is fully described by specifying the penumbral radius and the umbral field strength. Since the sunspot is not completely round, we took the azimuthal averages of the intensity and polarizations around its center as functions of distance from the center to compare with the corresponding theoretical distributions. The penumbral radius was then determined from the observed intensity profile. The umbral field strength is known to be about 2800G from the MSO Stokes polarimeter (Shibasaki *et al.*, 1994). Using the theoretical relation between the magnetic field strength and the polarization given by Sakurai *et al.* (1995), we have produced the theoretically expected polarization as a function of the distance from the sunspot center, which is then compared with the azimuthal averages of the observed polarization. The observed polarizations were found to be systematically smaller than the theoretically expected ones. Figure 6 shows the comparison of the theoretical polarization and the observed polarization multiplied by a suitable k -factor in each case of raw data and stray-light-corrected data. The k -factor suitable for the stray-light-corrected data is 2.2 and that suitable for the raw data is 2.8. The difference indicates that the stray light is partly responsible for the depolarizations. We have also applied our stray-light correction algorithm to Stokes Q/I and U/I images, and determined the k -factor for the linear polarization in the same way as used for the determination of the k -factor for the circular polarization.

Table I summarizes all the k factors determined on three different days for linear and circular polarizations. The k factors determined from the raw data have larger values, and vary much more from day to day than the stray light corrected data. Thus we see that stray light makes trouble in calibrating magnetograph observations obtained on different days. On the other hand, the k factors determined from the stray-light-corrected data vary little from day to day. Thus our method of stray-light correction should allow calibrations of magnetograph observations in

TABLE I
Estimated k factors (k_v for circular polarization and k_q for linear polarization)

Time (UT)	ϵ	FWHM	k_v (raw)	k_q (raw)	k_v (corr.)	k_q (corr.)
18 Aug. 01:50	0.12	4.8''	3.3	2.2	2.2	1.4
18 Aug. 23:55	0.10	2.3''	2.8	1.6	2.2	1.3
20 Aug. 02:30	0.14	4.0''	3.2	2.5	2.4	1.7
Chosen value			3.2	2.2	2.2	1.4

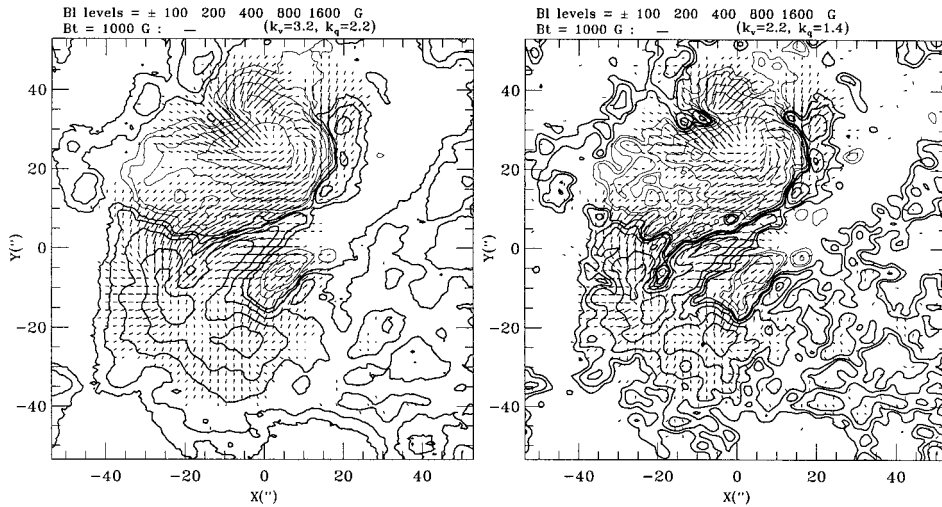


Figure 7. (a) Magnetic field map constructed from raw Stokes data. (b) Stray-light-corrected magnetic field map.

a consistent way, presumably, with an accuracy of 10% in both longitudinal and transverse field strengths.

Finally, we want to mention that stray-light correction is useful not only in the proper calibration of magnetic field strength in large sunspots, but also in better revealing small magnetic features. Figure 7 which compares two magnetic field maps illustrates this. Note that the raw magnetogram data and the restored data used different values of k for the proper calibration of field strengths in sunspots.

6. Summary

We have developed a method of stray-light correction which is applicable to filter-based magnetograph observations. The point spread function is determined from Stokes I images using either the limb profile method or the power spectrum method

as described in our previous work, and the observed Stokes images are deconvolved to produced stray-light-corrected images. We have devised an iterative algorithm for image deconvolution based on the maximum entropy principle. We found that our method is effective in correcting for stray light with a spread angle greater than the FWHM of the point spread function. We have examined the effect of stray light in the measurements of intensity and polarization in sunspots. As expected, a large and dark sunspot is more affected by large spread-angle stray light (scattering) and small sunspots are affected by both large and small spread-angle stray light. Stray light causes depolarization which varies from day to day especially in sunspots. We have found that our method of stray-light correction can correct for this kind of depolarization and enable magnetograph calibration in a stable way, with an accuracy of 10% in field strengths.

Appendix A. Derivation of Solution

Note that the discrete Fourier and inverse Fourier transforms are explicitly given by

$$X_n = \sum_s x_s \Theta_{ns} , \quad (22)$$

$$x_s = \frac{1}{N} \sum_n X_n \Theta_{ns}^* . \quad (23)$$

In the case of 2-dimensional discrete Fourier transforms, the Fourier kernels are given by $\Theta_{ns} = \exp(j2\pi(u_n i_s / N_x + v_n j_s / N_y))$ and $\Theta_{ns}^* = \exp(-j2\pi(u_n i_s / N_x + v_n j_s / N_y))$. N is the total number of data points given by the product $N_x N_y$. Here i_s and j_s are the coordinate indices of a data point in the spatial domain, and u_n and v_n are those in the Fourier domain. The solution x_s , or equivalently, X_n which maximizes H satisfies

$$\frac{\partial H}{\partial x_s} = 0 , \quad (24)$$

which, after the Fourier transform, results in

$$K_n = \alpha \sum_s a_s \log(z_s / m_s) \Theta_{ns} + Nc(X_n F_n - Y_N) F_n^* = 0 . \quad (25)$$

We determine the solution for this non-linear equation iteratively by using the Newton-Raphson approach. For this, we first evaluate the variation δK_n in terms of either δx_s or δX_n in the way

$$\delta K_n = \alpha \sum_s a_s^2 \delta x_s / z_s \Theta_{ns} + c |F_n|^2 \delta X_n \quad (26)$$

$$= (Nc |F_n|^2 + \alpha \eta) \delta X_n + \alpha \sum_s (a_s^2 / z_s - \eta) \delta x_s \Theta_{ns} \quad (27)$$

by introducing an arbitrary parameter η . We have found that an optimal value of η given by

$$\eta = \frac{\sum_s a_s^2 / z_s \delta x_s^2}{\sum_s \delta x_s^2} \quad (28)$$

can minimize the contribution of the second term, resulting in $\delta K_n \simeq (c |F_n|^2 + \alpha \eta) \delta X_n$. Thus, from the condition that

$$K_n^{(k+1)} = K_n^{(k)} + \delta K_n^{(k)} = 0, \quad (29)$$

it follows that

$$\delta X_n^{(k)} \simeq - \frac{K_n^{(k)} / Nc}{|F_n|^2 + \alpha \eta^{(k)} / Nc} \quad (30)$$

which leads to the iterative solution given by Equation (20) with $Q_n^{(k)} \equiv \sum_s a_s \log(z_s^{(k)} / m_s) \Theta_{ns} / Nc$ and $\lambda^{(k)} \equiv \eta^{(k)} / Nc$. If we set the dimensional constant c equal to $\sum_s a_s^2 / m_s$ which makes the dimensionless control parameter $\lambda^{(k)}$ of the order of unity, then we have

$$Q_n^{(k)} = \frac{N \sum_s a_s \log(z_s^{(k)} / m_s) \Theta_{ns}}{\sum_s a_s^2 / m_s}, \quad (31)$$

$$\lambda^{(k)} = \frac{N \sum_s a_s^2 / z_s (\delta x_s^{(k)})^2}{\sum_s a_s^2 / m_s \sum_s (\delta x_s^{(k)})^2}. \quad (32)$$

Appendix B. Numerical Algorithm

There are a couple of things to be considered in the numerical implementation of our algorithm. The one is how to calculate the control parameter $\lambda^{(k)}$ in each iteration step. The parameter depends on $\delta x_s^{(k)} \equiv x_s^{(k+1)} - x_s^{(k)}$ which is not known in advance, and it is what we should determine in the k -th iteration. For a calculation of $\lambda^{(k)}$, we use $\delta x_s^{(k-1)}$ which is already known instead of $\delta x_s^{(k)}$. This makes the calculation straightforward without the need of internal iteration. However, we

found that this approach sometimes makes the iterative process oscillate around a solution. To prevent this undesirable situation, we use for $\lambda^{(k)}$ the mean of the value determined in this way in the present step, and the value of the previous step.

The other thing to be considered is how to guarantee the positivity of the solution $z_s > 0$. Since the solution is searched in the Fourier domain, the positivity constraint is not automatically guaranteed. We handled this problem by picking up the weighted average of the solution obtained from Equation 20 and the solution in the previous step. The solution in the previous step is assumed to satisfy the positivity constraint; and the new solution also can be made to satisfy the constraint by choosing a suitable value of weighting factor.

We present the numerical algorithm as follows:

Step 1. Give a_s, b_s, m_s, y_s, f_s , and α as inputs.

Step 2. Calculate Y_n and F_n using Fourier transforms.

Step 3. Initialize: $k = 0, x_s^{(k)} = y_s, X_n^{(k)} = Y_n, \lambda^{(k)} = 1$.

Step 4. Calculate $Q_n^{(k)}$ using a Fourier transform (Equation (31)).

Step 5. Get $\delta X_n^{(k)}$ (Equation (30)).

Step 6. Calculate $\delta x_s^{(k)}$ using an inverse Fourier transform (Equation (23)).

Step 7. $\beta_1 = \min(z_s / \max((-a_s \delta x_s), 10^{-4} \max(m_s)), 1)$.

Step 8. $\beta = \min(0.9\beta_1, 1)$.

Step 9. Renew $x_s^{(k+1)} = x_s^{(k)} + \beta \delta x_s^{(k)}$ and $X_n^{(k+1)} = X_n^{(k)} + \beta \delta X_n^{(k)}$.

Step 10. Renew $\delta x_s^{(k)} = x_s^{(k+1)} - x_s^{(k)}$.

Step 11. Calculate λ^* (Equation (32)).

Step 11. $\lambda^{(k+1)} = (\lambda^* + \lambda^{(k)})/2$.

Step 12. Check convergence.

Step 13. If not converged, $k = k + 1$ and go to Step 4.

Note that this iteration scheme requires the calculation of 2 Fourier transforms in each iteration step whereas most maximum entropy method algorithms require 4–6 Fourier transforms (Cornwell and Evans, 1985; Hollis, Dorband, and Yusef-Zadeh, 1992; Nuñez and Llacer, 1993). Moreover, the convergence is fast enough because the search for the solution is done in the Fourier domain. We found from experiments that the deconvolution of solar images are satisfactorily achieved within about 10 iterations.

Finally, we discuss how to determine the regularizing parameter α . As mentioned earlier, if α has a very small value, then the likelihood term becomes much more important than the entropy term. Therefore, α must depend on the signal-to-noise ratio in the data. The similarity of the formal solution to the Wiener filter suggests that α which should be order of the ratio of noise power to the signal power is effective in suppressing artifacts while keeping real features. Thus in most observations α should have a value in the range $10^{-1} - 10^{-3}$. We have chosen $\alpha = 10^{-2}$ for the images presented in this work.

Acknowledgements

We are grateful to Y. Nishino, K. Shinoda, and M. Noguchi for their support during observations. One of us (J. Chae) would like to express his sincere thanks to T. Sakurai, K. Ichimoto, and Y. Suematsu for their hospitality given to him during his stay at Mitaka. We thank Martin Woodard and Carsten Denker for careful manuscript reading and good comments. The present work is supported in part by the Korea–China Cooperative Science Program (966–0203–005–2) and in part by the Basic Research Institute Program, Ministry of Education, ROK, 1997 (BSRI-97–5408). This work is partially supported by NSF under grant ATM-9628862 and NASA under grant NAG5-3536 to BBSO.

References

- Brault, J. W. and White, O. R.: 1971, *Astron. Astrophys.* **13**, 169.
- Chae, J., Yun, H. S., Sakurai, T., and Ichimoto, K.: 1998, *Solar Phys.* **183**, 229 (this issue, Paper I).
- Cornwell, T. J. and Evans, K. F.: 1985, *Astron. Astrophys.* **143**, 77.
- Gary, G. A., Hagyard, M. J., and West, E. A.: 1991, in L. J. November (ed.) *Solar Polarimetry*, National Solar Observatory, Sacramento Peak, p. 65.
- Gull, S. F.: 1989, in J. Skilling (ed.), *Maximum Entropy and Bayesian Methods*, Kluwer Academic Publishers, Dordrecht, Holland, p. 53.
- Hollis, J. M., Dorband, J. E., and Yusef-Zadeh, F.: 1992, *Astrophys. J.* **386**, 293.
- Högbom, J. A.: 1974, *Astron. Astrophys. Suppl. Ser.* **15**, 417.
- Lucy, L. B.: 1974, *Astron. J.* **79**, 745.
- Maltby, P.: 1992, in J. H. Thomas and Weiss N. O. (eds.), *Sunspots: Theory and Observations*, Kluwer Academic Publishers, Dordrecht, Holland, p. 103.
- Martínez Pillet, V.: 1992, *Solar Phys.* **140**, 207.
- Narayan, R. and Nityananda, R.: 1986, *Ann. Rev. Astron. Astrophys.* **24**, 127.
- Nityananda, R. and Narayan, R.: 1983, *Astron. Astrophys.* **118**, 194.
- Nuñez, J. and Llacer, J.: 1993, *Publ. Astron. Soc. Pacific* **105**, 1192.
- Richardson, W. H.: 1972, *J. Opt. Soc. Amer.* **62**, 55.
- Sakurai, T. et al.: 1995, *Publ. Astron. Soc. Pacific* **47**, 81.
- Shibasaki, K. et al.: 1994, *Publ. Astron. Soc. Pacific* **46**, L17.
- Skilling, J.: 1989, in J. Skilling (ed.), *Maximum Entropy and Bayesian Methods*, Kluwer Academic Publishers, Dordrecht, Holland, p. 45.
- Skilling, J.: 1990, in Pougere, P. F. (ed.), *Maximum Entropy and Bayesian Methods*, Kluwer Academic Publishers, Dordrecht, Holland, p. 341.
- Skilling, J. and Bryan, R. K.: 1984, *Monthly Notices Royal Astron. Soc.* **211**, 111.
- Skumanich, A.: 1992, in J. H. Thomas and N. O. Weiss (eds), *Sunspots: Theory and Observations*, Kluwer Academic Publishers, Dordrecht, Holland, p. 121.
- Wittmann, A. and Wöhl, H.: 1975, *Solar Phys.* **44**, 231.